



A finite element variational multiscale method for computations of turbulent flow over an aerofoil

Birupaksha Pal¹ · Sashikumaar Ganesan¹

Published online: 17 June 2015

© Indian Institute of Technology Madras 2015

Abstract Numerical simulation of turbulent flows over different aerofoil configurations are presented in this paper. The incompressible fluid flow is described by the time-dependent incompressible Navier–Stokes equations. Further, a finite element variational multiscale method is used to simulate the turbulent flows. Computation over a cylinder and different variants of aerofoils are presented. The obtained numerical results demonstrate the capabilities of variational multiscale methods.

Keywords Turbulent flows · Incompressible Navier–Stokes · Multiscale method · Finite elements

1 Introduction

Simulations of incompressible fluid flows, in particular turbulent flows, are highly demanded in many applications for very many reasons. Turbulent flows are highly unsteady flows, which contain several flow scales and the velocity field is superimposed by random velocity fluctuations. Both the laminar and turbulent incompressible fluid flows are described by the Navier–Stokes equations (NSE), whereas flows with low viscosity and high inertial forces are classified as turbulent flows. In particular, the Reynolds number, which is the ratio of inertial forces to viscous forces, in the dimensionless form of the NSE is used to classify laminar

and turbulent flows. The analytical solution of the NSE is deficient, in particular, with regard to the turbulent flow regime. There exist no analytical solutions for turbulent flow even for a simple flow configuration, and therefore the numerical approach is the only viable option for the simulation of turbulent flows, see [1, 2]. Despite several advances made in computational fluid dynamics (CFD), accurate modeling of turbulent flows is still very challenging.

The numerical simulation of turbulent flows is performed using either the direct numerical simulation (DNS) or turbulent models such as Reynolds-averaged Navier–Stokes equations (RANS) or large eddy simulations (LES). Further details on RANS can be found in [3]. In DNS approach, the NSE are solved by resolving all flow scales without any additional modeling for turbulence. The flow scales in turbulent flows vary in size, and a very fine mesh is needed in order to resolve all small flow scales, in particular, up to the Kolmogorov length scale. The very fine mesh makes the DNS computationally unfeasible for most of the practical applications. Currently, LES is one of the popular approaches for turbulence modeling. In LES, the large flow scales are resolved by the computational mesh and the effect of the small flow scales are incorporated into the large scales by turbulent models. The traditional LES relies on a filter function to separate the resolved and unresolved scales. However, the filter function induces commutation error in LES. Moreover an appropriate choice of filter function itself is very challenging. General overviews of the classical LES procedure can be found in [4–7].

In this paper we consider a relatively new approach, the variational multiscale method (VMS), for the turbulence simulation of fluid flows over an aerofoil. The theoretical framework of the VMS method has been established in [8] and was further developed for problems in computational mechanics in [9]. VMS separates the flow scales into two

✉ Sashikumaar Ganesan
sashi@serc.iisc.in

Birupaksha Pal
birupaksha@nmsc.serc.iisc.ernet.in

¹ Numerical Mathematics and Scientific Computing, SERC,
Indian Institute of Science, Bangalore 560012, India

or three different scales, for e.g., resolved large scale and unresolved small scale in a two level separation, and the scales are separated as resolved large scale, resolved small scale and unresolved small scale, in case of a three level separation. The flow scale separation enables to treat different flows scales with tailor-made numerical schemes. Two important aspects that characterize the VMS methods are: (i) variational projection is used to separate flow scales that avoids the use of filter function as in traditional LES thereby doing away with the commutation errors involved, and (ii) the influence/effect of the unresolved scales is incorporated into the resolved small scales and does not directly influence the resolved large scales. But due to the coupling of the scales, the resolved large scales are indirectly influenced by the modelling of the unresolved scales with the direct effect confined to the resolved small scales, see [10–15] for an overview, and [16] for an error analysis of one the schemes.

The paper is organized as follows. The mathematical model and the variational form of the incompressible fluid flows are presented in Sect. 2. After that a brief description of turbulence model including DNS and LES are presented in Sect. 3. A detailed description of the 3 scale VMS is presented in Sect. 4. The numerical results are presented in Sect. 5.

2 Mathematical model

2.1 Governing equations

We consider an incompressible fluid flow over an aerofoil in a two-dimensional channel, see Fig. 1 for a schematic view. The incompressible fluid flow in $(0, T] \times \Omega$ is described by the time-dependent incompressible NSE:

$$\frac{\partial \mathbf{u}}{\partial t} - \frac{2}{\text{Re}} \nabla \cdot \mathbb{D}(\mathbf{u}) + (\mathbf{u} \cdot \nabla) \mathbf{u} + \nabla p = \mathbf{0}, \quad \nabla \cdot \mathbf{u} = 0, \quad (1)$$

where Ω is a bounded domain $\Omega \subset \mathbb{R}^2$ and T is a given final time. The NSE are closed with the initial condition

$$\mathbf{u}(0, \cdot) = \mathbf{u}_0 \quad \text{in } \Omega$$

and boundary conditions

$$\begin{aligned} \mathbf{u}(t, \mathbf{x}) &= \mathbf{u}_D && \text{on } (0, T] \times \Gamma_{in}, \\ \mathbf{u}(t, \mathbf{x}) &= \mathbf{0} && \text{on } (0, T] \times \Gamma_{wall}, \\ \left(\frac{2}{\text{Re}} \mathbb{D}(\mathbf{u}) - p \mathbb{I} \right) \cdot \mathbf{n} &= \mathbf{0} && \text{on } (0, T] \times \Gamma_{out}. \end{aligned}$$

Here, \mathbf{u} is the fluid velocity, p is the pressure, t is the time, \mathbf{u}_0 is a given initial velocity, \mathbf{u}_D is a given inlet velocity, \mathbb{I} is the identity tensor and \mathbf{n} is the outward normal to the

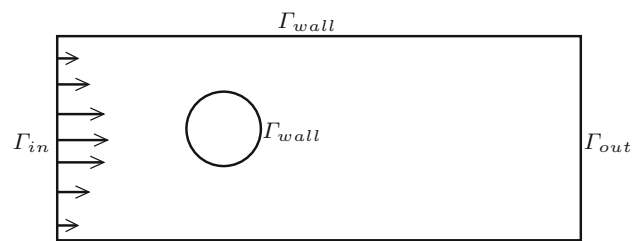


Fig. 1 Computational domain for a fluid flow over an obstacle

boundary Γ_{out} . Further, the velocity deformation tensor and the Reynolds number are defined by

$$\mathbb{D}(\mathbf{u}) = \frac{\nabla \mathbf{u} + \nabla \mathbf{u}^T}{2} \quad \text{and} \quad \text{Re} = \frac{\rho U L}{\mu},$$

where ρ is the density of the fluid, μ is the dynamic viscosity, U and L are characteristic velocity and length scales, respectively.

2.2 Variational form

Let $L^2(\Omega)$, $H^1(\Omega)$ and $(\cdot, \cdot)_\Omega$ be the standard Sobolev spaces and the inner product in $L^2(\Omega)$ and its vector-valued versions, respectively. Further, the velocity and pressure spaces are defined as

$$V := \{ \mathbf{v} \in H^1(\Omega)^2 : \mathbf{v} = \mathbf{0} \text{ on } \Gamma_{in} \cup \Gamma_{wall} \}, \quad Q := L^2(\Omega).$$

Now multiplying the momentum and mass balance equations in (1) with test functions $\mathbf{v} \in V$ and $q \in Q$, respectively, and integrate over Ω . After applying the Gaussian theorem for the integrals containing the deformation tensor, and incorporating all boundary conditions, the weak form of the NSE (1) read:

For given \mathbf{u}_0 and \mathbf{u}_D , find $(\mathbf{u}, p) \in V \times Q$ such that

$$\left(\frac{\partial \mathbf{u}}{\partial t}, \mathbf{v} \right) + a(\mathbf{u}, \mathbf{u}, \mathbf{v}) - b(p, \mathbf{v}) + b(q, \mathbf{u}) = \mathbf{0} \quad (2)$$

for all $(\mathbf{v}, q) \in V \times Q$, where

$$\begin{aligned} a(\hat{\mathbf{u}}, \mathbf{u}, \mathbf{v}) &= \frac{2}{\text{Re}} \int_\Omega \mathbb{D}(\mathbf{u}), \mathbb{D}(\mathbf{v}) \, dx \\ &\quad + \int_\Omega (\hat{\mathbf{u}} \cdot \nabla) \mathbf{u} \cdot \mathbf{v} \, dx, \\ b(q, \mathbf{v}) &= \int_\Omega q \nabla \cdot \mathbf{v} \, dx. \end{aligned}$$

3 Turbulent flow models

Turbulent flows are generally characterized by chaotic behavior in the flow dynamics. In common parlance, flows with high Reynolds number are considered to be turbulent. One of the main distinctive features of turbulent flows is

the presence of a multitude of scales. Even though several advances have been made in the field of computational fluid dynamics, handling different scales in a turbulent flow simulation is still challenging. Some of the popular methods for turbulent flow simulations are the DNS, LES and more recently the VMS. We briefly discuss these methods in the next sections.

3.1 Direct numerical simulation

Numerical simulation is the only practical way out for the solution of turbulent flow problems since analytical solution is impossible to obtain. As mentioned before, capturing all flow scales in turbulent flow simulations is the most challenging task. The most straight-forward approach is to resolve all scales, in particular up to the Kolmogorov length scale, by the computational mesh. This approach is the DNS. This approach has two serious limitations: (i) high computational cost incurred due to a high resolution mesh and (ii) the effects of small scales that are not captured by the computational mesh (unresolved small scales) are lost since no modelling or approximation are involved to incorporate the effects of unresolved small scales. Further, there is a complete dependence on the available computational capabilities. Nevertheless, the DNS is the most accurate approach if the computing power at disposal allows to use a fine mesh that resolves flow scales up to the Kolmogorov length scale. Moreover, DNS approach does not contain any numerical modeling terms.

3.2 Large eddy simulation

Another popular approach for numerical simulation of turbulent flow is the large eddy simulation [6, 7]. Contrary to the DNS, only the large scales are resolved by the computational mesh in the LES, whereas the effects of unresolved small scales on the flow dynamics are incorporated through a turbulence model. Since the LES mesh is coarser in comparison to the mesh used in DNS, LES is computationally inexpensive. In the LES approach, the separation of the flow scales into a large and small scales are performed using a filter function with some appropriately chosen filter width. One of the popular filters, often used in the LES approach is the Gaussian filter,

$$g_\delta(\mathbf{x}) = \frac{6^{d/2}}{\delta^2 \pi} \exp\left(-\frac{6}{\delta^2} \|\mathbf{x}\|_2^2\right),$$

where δ is the filter width and d is the dimension of the flow problem. The characteristic properties of filter functions are that they should be linear and commutative with respect to differentiation, which are required for the unbounded domains say \mathbb{R}^d .

After filtering the NSE (1) with an appropriate filter function, the filtered incompressible NSE in $(0, T] \times \mathbb{R}^d$ (an unbounded domain) become

$$\begin{aligned} \frac{\partial \bar{\mathbf{u}}}{\partial t} - \frac{2}{\text{Re}} \nabla \cdot \mathbb{D}(\bar{\mathbf{u}}) + \nabla \cdot (\bar{\mathbf{u}}\bar{\mathbf{u}}^T) + \nabla \bar{p} &= \mathbf{0}, \\ \nabla \cdot \bar{\mathbf{u}} &= 0, \end{aligned}$$

with $\bar{\mathbf{u}}(0, \cdot) = \bar{\mathbf{u}}_0$, where the bar in the above variables denotes that the variables are filtered with a filter function. Let $\mathbf{u} = \bar{\mathbf{u}} + \mathbf{u}'$ and $\mathbf{p} = \bar{p} + p'$ be a decomposition of the velocity and pressure respectively, into unresolved small scale (\mathbf{u}', p') and resolved large scale $(\bar{\mathbf{u}}, \bar{p})$. Further, using the linearity of the filter function $\overline{\mathbf{u} + \lambda \mathbf{v}} = \bar{\mathbf{u}} + \lambda \bar{\mathbf{v}}$, the decomposition of the nonlinear convective term can be written as:

$$\overline{\mathbf{u}\mathbf{u}^T} = \overline{\bar{\mathbf{u}}\bar{\mathbf{u}}^T} + \overline{\bar{\mathbf{u}}\mathbf{u}'^T} + \overline{\mathbf{u}'\bar{\mathbf{u}}^T} + \overline{\mathbf{u}'\mathbf{u}'^T}.$$

Applying these decompositions leads to the space averaged NSE:

$$\begin{aligned} \frac{\partial \bar{\mathbf{u}}}{\partial t} - \frac{2}{\text{Re}} \nabla \cdot \mathbb{D}(\bar{\mathbf{u}}) + \nabla \cdot (\overline{\mathbf{u}\mathbf{u}^T}) + \nabla \cdot \mathbb{T}(\mathbf{u}, \mathbf{u}) + \nabla \bar{p} &= \mathbf{0} \\ \text{in } (0, T] \times \mathbb{R}^d \\ \nabla \cdot \bar{\mathbf{u}} &= 0 \quad \text{in } (0, T] \times \mathbb{R}^d \end{aligned}$$

with $\bar{\mathbf{u}}(0, \cdot) = \bar{\mathbf{u}}_0$. Here

$$\mathbb{T}(\mathbf{u}, \mathbf{u}) = \overline{\mathbf{u}\mathbf{u}^T} - \overline{\bar{\mathbf{u}}\bar{\mathbf{u}}^T} = \overline{\bar{\mathbf{u}}\mathbf{u}'^T} + \overline{\mathbf{u}'\bar{\mathbf{u}}^T} + \overline{\mathbf{u}'\mathbf{u}'^T}$$

is known as ‘‘Reynolds stress tensor’’. In the above equations, the stress tensor term gives rise to a ‘‘closure problem’’, and thus it needs to be modeled or approximated. One of the most commonly used model for the stress tensor term is the Smagorinsky eddy viscosity model,

$$\mathbb{T}(\mathbf{u}, \mathbf{u}) - \frac{\text{tra } \mathbb{T}(\mathbf{u}, \mathbf{u})}{3} \mathbb{I} = -2\nu_T \mathbb{D}(\bar{\mathbf{u}}),$$

where ν_T is the turbulent viscosity given by

$$\nu_T = \nu_S \|\mathbb{D}\| = c_S \delta^2 \|\mathbb{D}(\bar{\mathbf{u}})\|.$$

Some of the other popular models proposed in the literature are the dynamic subgrid scale model, Taylor LES model, second order and fourth order rational LES model, see [17] for further details.

4 Variational multiscale method (VMS)

The variational multiscale method for turbulent flows is also based on the decomposition of the flow scales into resolved and unresolved scales. But unlike the application of a filter function in LES, scale separation in VMS is

realized in a different way, for example using projection into appropriate spaces. The resolved scales are captured by a standard finite element space, whereas the unresolved scales, also known as the sub-grid scale field, are modeled [18–20]. Moreover, the resolved scales can further be separated into resolved large and resolved small scales [10, 13, 21, 22].

In this work, the three-scale VMS is considered. Let $\mathbf{u} = \bar{\mathbf{u}} + \tilde{\mathbf{u}} + \hat{\mathbf{u}}$ and $p = \bar{p} + \tilde{p} + \hat{p}$ (3)

be the decomposition of the unknowns into resolved large $(\bar{\mathbf{u}}, \bar{p})$, resolved small $(\tilde{\mathbf{u}}, \tilde{p})$ and unresolved small scales $(\hat{\mathbf{u}}, \hat{p})$, respectively. Further, consider a direct sum decomposition of V and Q as

$$V = \bar{V} \oplus \tilde{V} \oplus \hat{V} \quad \text{and} \quad Q = \bar{Q} \oplus \tilde{Q} \oplus \hat{Q} \quad (4)$$

where (\bar{V}, \bar{Q}) denotes the resolved large scale spaces, (\tilde{V}, \tilde{Q}) the resolved small scale spaces, and (\hat{V}, \hat{Q}) the unresolved small scale spaces. For simplicity, we denote the variational form (2) as

$$\left(\frac{\partial \mathbf{u}}{\partial t}, \mathbf{v} \right) + A(\mathbf{u}; (\mathbf{u}, p); (\mathbf{v}, q)) = \mathbf{0}, \quad (5)$$

where

$$A(\hat{\mathbf{u}}; (\mathbf{u}, p); (\mathbf{v}, q)) = a(\hat{\mathbf{u}}, \mathbf{u}, \mathbf{v}) - b(p, \mathbf{v}) + b(q, \mathbf{u}).$$

Using the decompositions (3) and (4), the variational form (5) can be written as a coupled system of equations, and it reads:

For given \mathbf{u}_0 and \mathbf{u}_D , find $(\bar{\mathbf{u}}, \bar{p}) \in \bar{V} \times \bar{Q}$, $(\tilde{\mathbf{u}}, \tilde{p}) \in \tilde{V} \times \tilde{Q}$, and $(\hat{\mathbf{u}}, \hat{p}) \in \hat{V} \times \hat{Q}$ such that

$$\left(\frac{\partial(\bar{\mathbf{u}} + \tilde{\mathbf{u}} + \hat{\mathbf{u}})}{\partial t}, \bar{\mathbf{v}} \right) + A(\mathbf{u}; (\bar{\mathbf{u}} + \tilde{\mathbf{u}} + \hat{\mathbf{u}}, \bar{p} + \tilde{p} + \hat{p}), (\bar{\mathbf{v}}, \bar{q})) = \mathbf{0} \quad (6)$$

$$\left(\frac{\partial(\bar{\mathbf{u}} + \tilde{\mathbf{u}} + \hat{\mathbf{u}})}{\partial t}, \tilde{\mathbf{v}} \right) + A(\mathbf{u}; (\bar{\mathbf{u}} + \tilde{\mathbf{u}} + \hat{\mathbf{u}}, \bar{p} + \tilde{p} + \hat{p}), (\tilde{\mathbf{v}}, \tilde{q})) = \mathbf{0} \quad (7)$$

$$\left(\frac{\partial(\bar{\mathbf{u}} + \tilde{\mathbf{u}} + \hat{\mathbf{u}})}{\partial t}, \hat{\mathbf{v}} \right) + A(\mathbf{u}; (\bar{\mathbf{u}} + \tilde{\mathbf{u}} + \hat{\mathbf{u}}, \bar{p} + \tilde{p} + \hat{p}), (\hat{\mathbf{v}}, \hat{q})) = \mathbf{0} \quad (8)$$

for all $(\bar{\mathbf{v}}, \bar{q}) \in \bar{V} \times \bar{Q}$, $(\tilde{\mathbf{v}}, \tilde{q}) \in \tilde{V} \times \tilde{Q}$, $(\hat{\mathbf{v}}, \hat{q}) \in \hat{V} \times \hat{Q}$, and for each $t \in [0, T]$. In the above system (6)–(8), the following assumptions are made:

- The equation with the test functions from the unresolved scales, (8), is ignored, as the unresolved small scales cannot be captured numerically
- Unresolved scales $(\hat{\mathbf{v}}, \hat{q})$ do not influence the resolved large scales directly, that is, the interaction between $(\hat{\mathbf{u}}, \hat{p})$ and $(\bar{\mathbf{v}}, \bar{q})$ is ignored in the equation (6)

- The effect of the unresolved scales on the resolved small scales is modeled by an appropriate turbulence model, that is,

$$\left(\frac{\partial \hat{\mathbf{u}}}{\partial t}, \tilde{\mathbf{v}} \right) + A(\mathbf{u}; (\hat{\mathbf{u}}, \hat{p}), (\tilde{\mathbf{v}}, \tilde{q})) \approx B(\mathbf{u}; (\bar{\mathbf{u}}, \bar{p}), (\tilde{\mathbf{u}}, \tilde{p}), (\tilde{\mathbf{v}}, \tilde{q})),$$

where the Smagorinsky eddy viscosity model is used in computations.

Using these assumptions, the three-level variational multiscale scheme for the NSE reads:

For given \mathbf{u}_0 and \mathbf{u}_D , find $(\bar{\mathbf{u}}, \bar{p}) \in \bar{V} \times \bar{Q}$, and $(\tilde{\mathbf{u}}, \tilde{p}) \in \tilde{V} \times \tilde{Q}$ such that

$$\left(\frac{\partial(\bar{\mathbf{u}} + \tilde{\mathbf{u}})}{\partial t}, \bar{\mathbf{v}} \right) + A(\bar{\mathbf{u}} + \tilde{\mathbf{u}}; (\bar{\mathbf{u}} + \tilde{\mathbf{u}}, \bar{p} + \tilde{p}), (\bar{\mathbf{v}}, \bar{q})) = \mathbf{0} \quad (9)$$

$$\left(\frac{\partial(\bar{\mathbf{u}} + \tilde{\mathbf{u}})}{\partial t}, \tilde{\mathbf{v}} \right) + A(\bar{\mathbf{u}} + \tilde{\mathbf{u}}; (\bar{\mathbf{u}} + \tilde{\mathbf{u}}, \bar{p} + \tilde{p}), (\tilde{\mathbf{v}}, \tilde{q})) + B(\bar{\mathbf{u}} + \tilde{\mathbf{u}}; (\bar{\mathbf{u}}, \bar{p}), (\tilde{\mathbf{u}}, \tilde{p}), (\tilde{\mathbf{v}}, \tilde{q})) = \mathbf{0} \quad (10)$$

Unlike the two-scale VMS and the LES, the turbulence model in three-scale VMS acts only on the resolved small scale. However, it indirectly affects the resolved large scales due to the inherent coupling of the resolved small scales with the resolved large scales. Moreover, in order to capture the resolved small scales, the finite element for $(\tilde{\mathbf{u}}, \tilde{p})$ has to be rich enough in comparison to the finite element space of $(\bar{\mathbf{u}}, \bar{p})$. It can be realized in two ways: (i) bubble based VMS [23] i.e., choosing a standard finite element space for $(\bar{\mathbf{u}}, \bar{p})$, and enrich the same space with polynomial bubble functions for $(\tilde{\mathbf{u}}, \tilde{p})$, and (ii) projection based VMS [24], i.e., choosing two different finite element spaces for $(\tilde{\mathbf{u}}, \tilde{p})$ and $(\bar{\mathbf{u}}, \bar{p})$. In this paper we use a projection based VMS.

4.1 Discrete form

We first present the temporal discretization and then a finite element discretization for the projection based VMS model of the NSE (9) and (10). Let $0 = t_0 < t_1 < \dots < t_N = T$ be a decomposition of the considered time interval $[0, T]$ and $\delta t = t_{n+1} - t_n$, $n = 0, \dots, N - 1$, be the uniform time step. Further, we use short notation $\mathbf{u}^n(\mathbf{x}) = \mathbf{u}(t^n, \mathbf{x})$ to denote the function value at time t_n . In computation, the second order Crank–Nicolson method is used for the temporal discretization. We next discuss the spatial discretization. Let Ω_h be a triangulation of the domain Ω into cells, where h denotes the maximum diameter among all cells in the triangulation. Let $V_h \subset V$ and $Q_h \subset Q$ to be two conforming finite element (finite dimensional) spaces satisfying the inf-sup condition

$$\inf_{q_h \in Q_h} \sup_{\mathbf{v}_h \in V_h} \frac{(\nabla \cdot \mathbf{v}_h, q_h)}{\|\nabla \mathbf{v}_h\|_{L^2} \|q_h\|_{L^2}} \geq \beta > 0 \tag{11}$$

i.e., for some positive constant β that is independent of the mesh parameter h . The Taylor-Hood finite element pair P_2/P_1 i.e., continuous piecewise quadratic and continuous piecewise linear polynomials for the velocity and pressure, respectively, satisfies the inf-sup condition on triangles. Further, let $W := L^2(\Omega)^{d \times d}$ be a space of $d \times d$ symmetric tensors, that is,

$$W := \left\{ \mathbb{W} \in L^2(\Omega)^{d \times d} : \mathbb{W} = \mathbb{W}^T \right\}.$$

Let $W_H \subset W$ and further let, $P_{W_H} : W \rightarrow W_H$ be a L^2 -projection from W to W_H .

On the application of the Crank–Nicolson and the finite elements for the temporal discretization and spatial discretization, respectively, the projection based VMS discrete form of the NSE in the time interval (t^n, t^{n+1}) read:

For given \mathbf{u}_D and \mathbf{u}^n with $\mathbf{u}^0 = \mathbf{u}_0$, find $\mathbf{u}_h^{n+1} \in V_h$, $p_h^{n+1} \in Q_h$ and $P_{W_H} \mathbb{D}(\mathbf{u}_h^{n+1}) \in W_H$ such that

$$\begin{aligned} & (\mathbf{u}_h^{n+1} - \mathbf{u}_h^n, \mathbf{v}_h) + \frac{\delta t}{2} [a(\mathbf{u}_h^{n+1}, \mathbf{u}_h^{n+1}, \mathbf{v}) - b(p_h^{n+1}, \mathbf{v}) \\ & + (v_T(\mathbb{I} - P_{W_H})\mathbb{D}(\mathbf{u}_h^{n+1}), \mathbb{D}(\mathbf{v}_h))] \\ & = \frac{\delta t}{2} [a(\mathbf{u}_h^n, \mathbf{u}_h^n, \mathbf{v}) - b(p_h^n, \mathbf{v}) \\ & + (v_T(\mathbb{I} - P_{W_H})\mathbb{D}(\mathbf{u}_h^n), \mathbb{D}(\mathbf{v}_h))] \end{aligned} \tag{12}$$

$$b(q, \mathbf{u}_h^{n+1}) = 0 \tag{13}$$

$$((\mathbb{I} - P_{W_H})\mathbb{D}(\mathbf{u}_h^{n+1}), \mathbb{W}_H) = 0 \tag{14}$$

for all $(\mathbf{v}_h, q_h) \in V_h \times Q_h$ and $\mathbb{W}_H \in W_H$.

Remark 1 The equation (14) represents a L^2 projection from W onto W_H . In three-scale VMS, the space V_h contains functions that resolve both the large and the small scales, whereas the space W_H can be thought to be representing the large scales of the flow. The main difference between the VMS method and the traditional LES is the scale separation. In the VMS, the scale separation is done by a projection onto appropriate spaces instead of filtering using filter function, thereby doing away with the complications arising out of it. Moreover, instead of L^2 projection, other kinds of projections can also be used. For a more detailed discussion on the various projection operators the reader is referred to [25].

Remark 2 The large scale space W^H and the additional turbulent model v_T have to be chosen suitably, and the choice of these two determines the turbulence modelling of the scheme. A popular choice for the turbulent viscosity model is the Smagorinsky eddy viscosity model. The first equation (12) essentially means that the turbulent viscosity is added to all resolved scales, and then it is subtracted from the large scales, thereby limiting the effects of the unresolved small scale only on the resolved small scales. This is the main idea of the VMS [24].

Fig. 2 Pressure contours in the fluid flow over a circular cylinder at different instances $t = 5, 10, 15, 20$

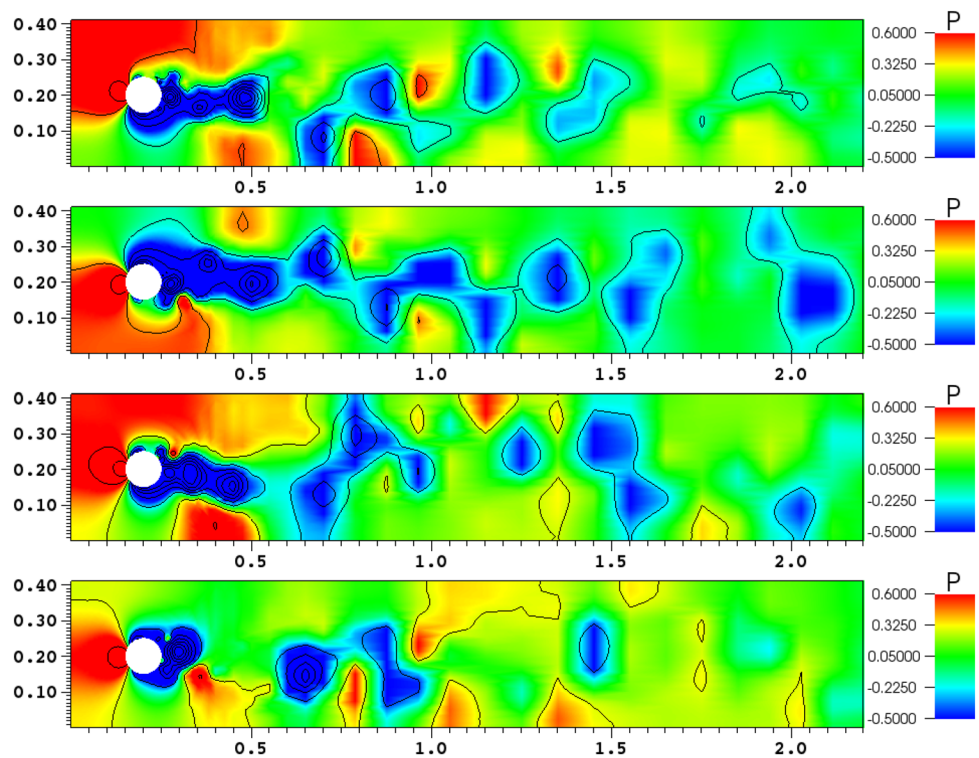


Fig. 3 Tangential velocity (x-axis) contours in the fluid flow over a circular cylinder at different instances $t = 5, 10, 15, 20$

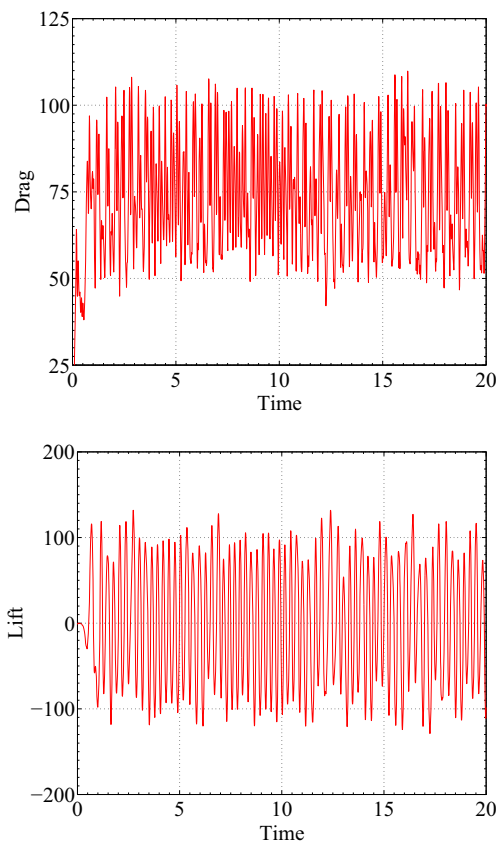
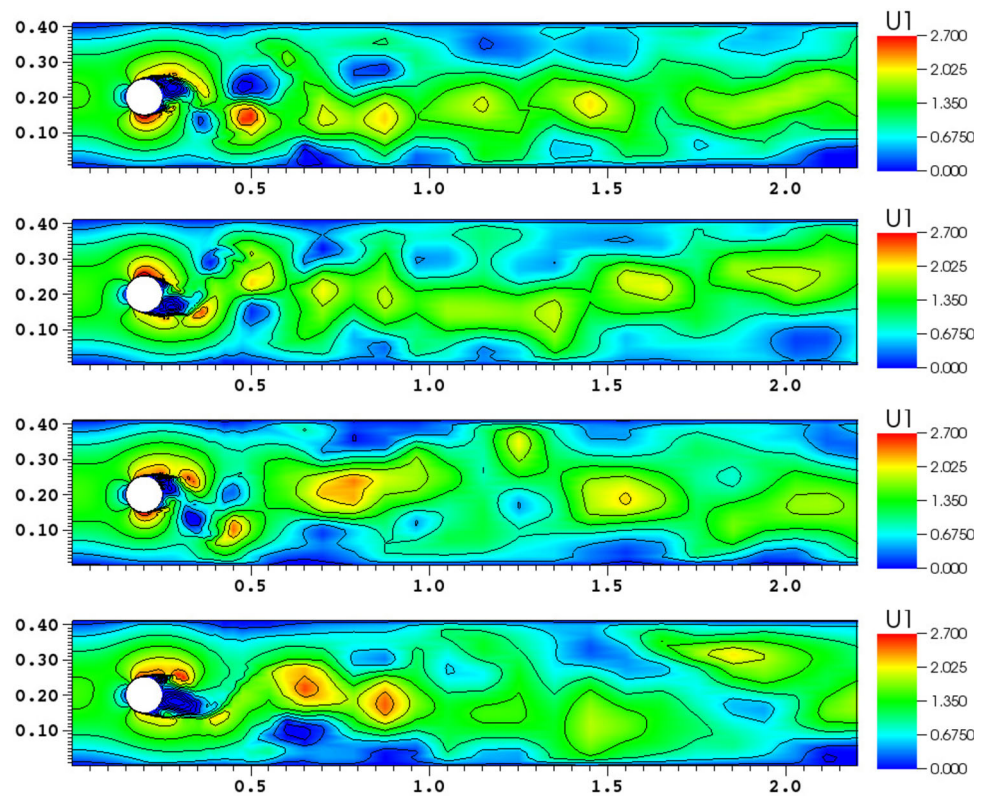


Fig. 4 The drag and lift over time for a flow over a circular cylinder

Remark 3 The important aspect of implementation of the scheme is the choice of the space for large scale. There are broadly two ways of defining the large scale space W_H , the first one is to define W_H on a coarser grid than that of (V_h, Q_h) , and the second approach is to define W_H on the same grid of (V_h, Q_h) , but using lower order polynomials for W_H and higher order polynomials for (V_h, Q_h) . In computations we chose the latter with W_H as a discontinuous finite element space with L^2 orthogonal basis, as it can be efficiently implemented with minor changes in an already existing finite element code. For a detailed description of the algorithm the reader is referred to [24].

5 Numerical results

In this section, we first present the numerical results for a flow over a cylinder in a rectangular channel using the three-scale VMS described in the previous section. The numerical results are compared with the results proposed in the literature. After that flows over two different aerofoils (i) NACA 24012, and (ii) SD7003 in a channel are considered. A rectangular channel $\Omega := (0, 4.1) \times (0, 2.2)$ and a steady state parabolic inflow profile $\mathbf{u}_D = (u_{in}, 0)$ with $u_{in} = 6y(1 - y)$ is used for the flow over a cylinder example. For the two examples on the flow over aerofoils of different

shapes, our chosen dimensions for the channel is $\Omega := (0, 6.2) \times (1.5, 2.5)$ with the steady parabolic inflow profile $\mathbf{u}_D = (u_{in}, 0)$ with $u_{in} = 4y(1 - y)$. All computations are performed until the end time $T = 20$ with $\delta t = 0.01$ and $Re = 66667$. Moreover, the Smagorinsky turbulence model for the turbulent viscosity, $\nu_T = \nu_S \|\mathbb{D}\| = c_S \delta^2 \|\mathbb{D}(\bar{\mathbf{u}})\|_F$, with $c_S = 0.01$, the filter width, $\delta = 0.02$ is used. Further, the Frobenius norm, $\|\cdot\|_F$ is used to calculate the norm of the deformation tensor.

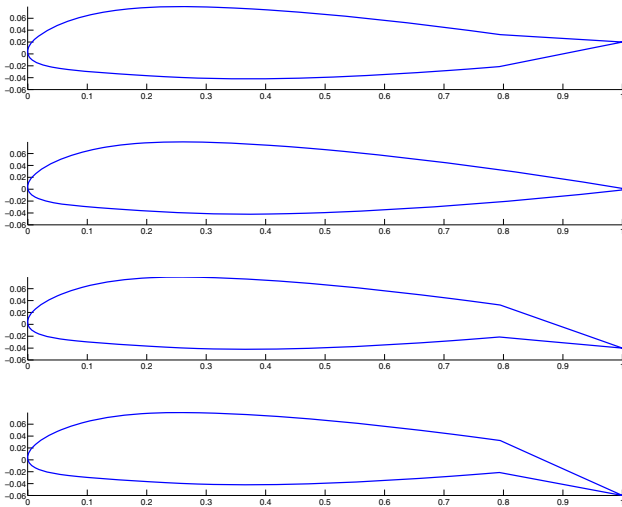
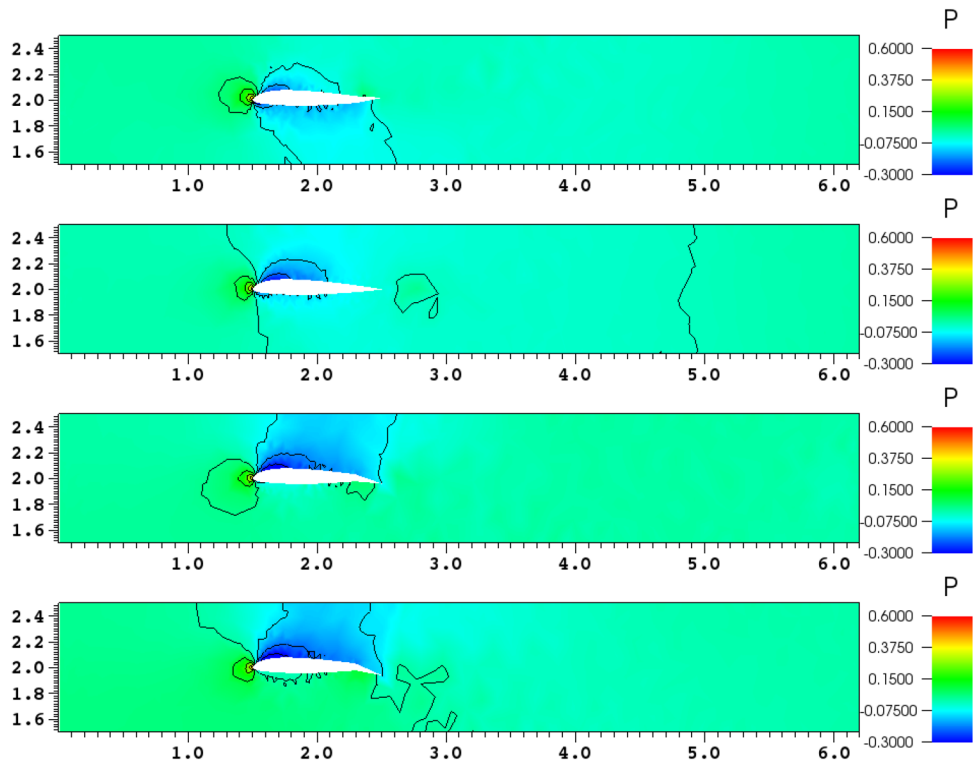


Fig. 5 Shapes of different variants of NACA24012 airfoil

Fig. 6 Pressure contours in the fluid flow over different variants of NACA24012 airfoil at $t = 10$. Top to bottom Var. 1–4



5.1 Flow over a 2D circular cylinder

In the first test example, we consider a circular cylinder of radius 0.05 units placed inside the channel at (0.2, 1.1). The choice of Taylor-Hood finite element pair P_2/P_1 for the velocity and pressure, results in 27,232 degrees of freedom (DOF) for the velocity and 3480 DOF for the pressure.

The computationally obtained pressure and velocity contours at different instances $t = 5, 10, 15, 20$ are depicted in Figs. 2 and 3, respectively. The flow profile conforms with the standard high Reynolds number flow calculations over cylinder. The contours in the Fig. 3, represent the vorticity in the wake of the cylinder. Further, the drag and lift induced by the flow on the cylinder are depicted in Fig. 4. The observed oscillations in the drag and lift coefficients are consistent with the numerical results in the literature [24].

5.2 Flow over an aerofoil NACA 24012

We next consider flow over an aerofoil in a rectangular channel. The standard NACA24012 aerofoil is considered, and its coordinates are obtained using NACA 5 digit airfoil generator. The tip of the aerofoil is positioned at (1.5, 2) in the channel. Moreover, four variants of the NACA24012 aerofoil are considered by varying the tail position of the aerofoil. The considered variants are (i) tail-up, tip of the

Fig. 7 Tangential velocity (x-axis) contours in the fluid flow over different variants of NACA24012 aerofoil at $t = 10$. Top to bottom Var. 1–4

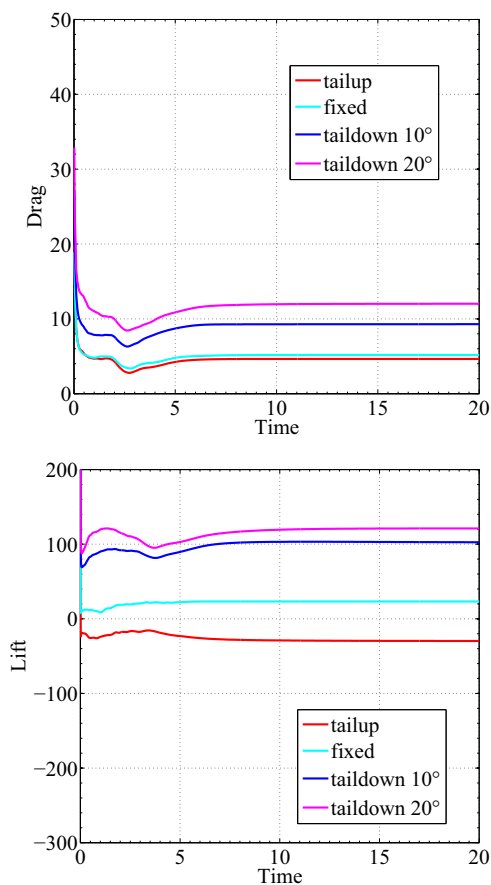
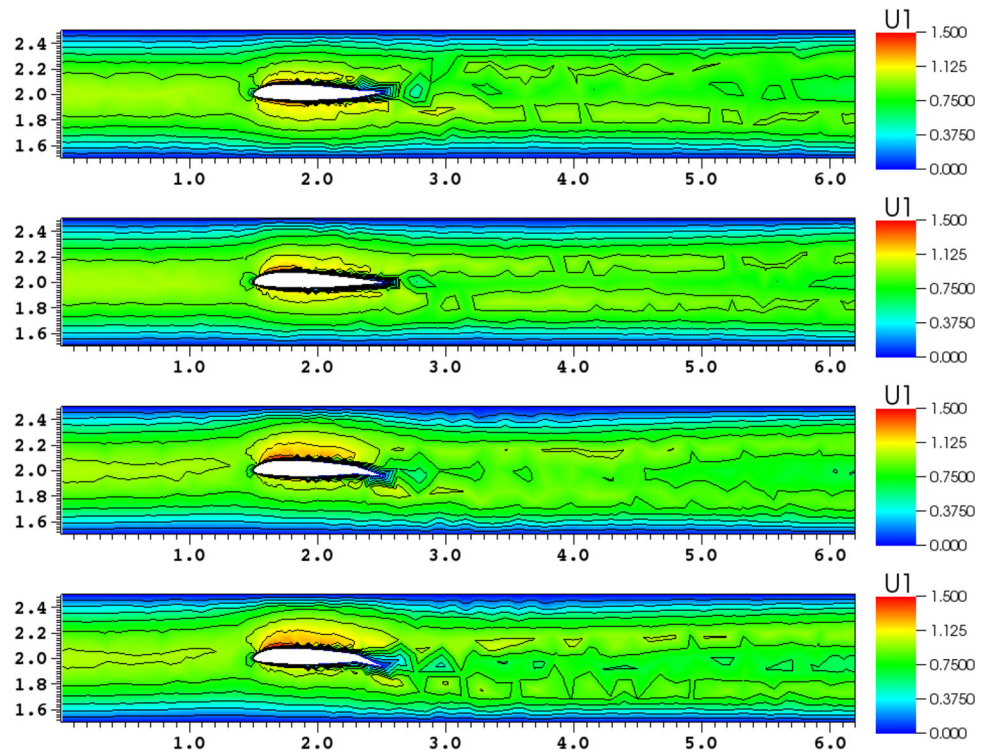


Fig. 8 The drag and the lift generated by the flow over different variants of the NACA24012 aerofoil

tail positioned at (2.5, 2.02), (ii) standard NACA24012 configuration, (iii) tail-down with tip of the tail positioned at (2.5, 1.96), and (iv) tail-down with tip of the tail positioned at (2.5, 1.94). The shapes of all these four variants of NACA24012 aerofoil are shown in Fig. 5.

The variation in the position of the tail induces changes in the behavior of the flow dynamics. The computationally obtained pressure contours in all four variants of the aerofoil at the dimensionless time $t = 10$ are depicted in Fig. 6. The pressure distribution under the aerofoil is negative in the variant 1 due to the upward position of the tail. As expected, the pressure value is positive under the aerofoil in all other variants. Further, the pressure value over the aerofoil becomes more and more negative when the position of the tail comes down. Next, the contours of the tangential velocity (x-axis) at the dimensionless time $t = 10$ are depicted in Fig. 7. It can clearly be seen that the flow dynamics changes when the position of the tail is altered. Moreover, the vorticity is not observed for the used value of the Reynolds number in the considered flow configuration. Next, the drag and the lift generated by the flow over different variants of the NACA24012 aerofoil are present in Fig. 8. The drag coefficient in variant 1 and 2 are more or the same, whereas the drag increases when the position of the tail comes down. As expected, the lift coefficient is negative in the variant 1 due to tail-up position in the aerofoil. However, the lift coefficient increases when the tail of the aerofoil is lowered, see Fig. 8.

5.3 Flow over an aerofoil SD7003

In the final result that we present, we consider the simulation of the flow over another variant of aerofoil, the SD7003 aerofoil in a rectangular channel of the same geometry as in the previous example. The surface coordinates of the aerofoil are obtained from the UIUC Airfoil Coordinates Database. For the purpose of continuity and comparison, we conduct a set of similar computations as in

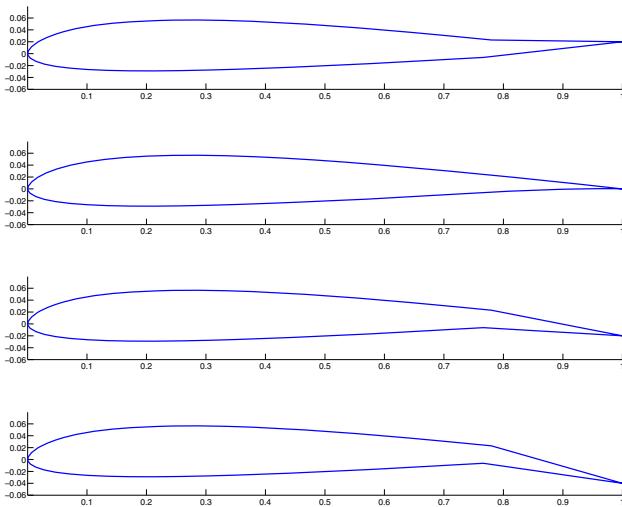
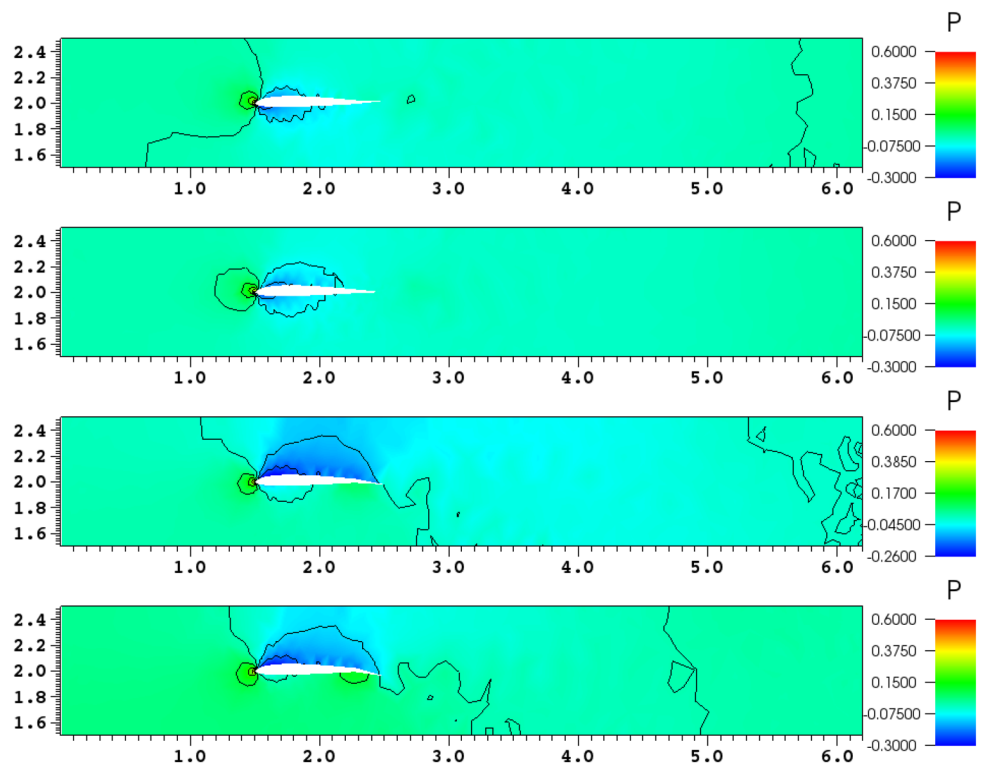


Fig. 9 Shapes of different variants of SD 7003 aerofoil

Fig. 10 Pressure contours in the fluid flow over different variants of SD 7003 aerofoil at $t = 10$. Top to bottom Var. 1–4



the previous one. The tip of the aerofoil is positioned at (1.5, 2) and (i) tail-up, tip of the tail positioned at (2.5, 2.02), (ii) standard SD7003 configuration, (iii) tail-down with tip of the tail positioned at (2.5, 1.98), and (iv) tail-down with tip of the tail positioned at (2.5, 1.96). Fig. 9 outlines these different shapes of the SD 7003 aerofoil.

Figure 10 depicts the computationally obtained pressure contours in all four variants of the aerofoil at the dimensionless time $t = 10$. The general behavior of the pressure and the velocity contours can be seen to be quite similar for both the aerofoils. The pressure distribution under the aerofoil is observed to be negative in the variant 1 due to the upward position of the tail. As expected, we can see the pressure value is positive under the aerofoil in all other variants. Moreover, as the tail is bend down, thereby increasing the camber, the pressure becomes more and more negative. The tangential velocity (x -axis) of the flow in all the four variants at $t = 10$, are depicted in Fig. 11.

The changes in the flow dynamics with altering of the tail position can easily be observed here. The drag and the lift generated by the flow over different variants of the SD 7003 aerofoil are present in Fig. 12. The drag coefficient in the variant 1 and 2 are similar, whereas the drag increases when the position of the tail comes down. As expected, the lift coefficient is observed to be negative in the variant 1 due to tail-up position in the aerofoil. However, the lift coefficient increases when the tail of the aerofoil is lowered, see Fig. 12.

Fig. 11 Tangential velocity (x -axis) contours in the fluid flow over different variants of SD 7003 aerofoil at $t = 10$. Top to bottom Var. 1–4

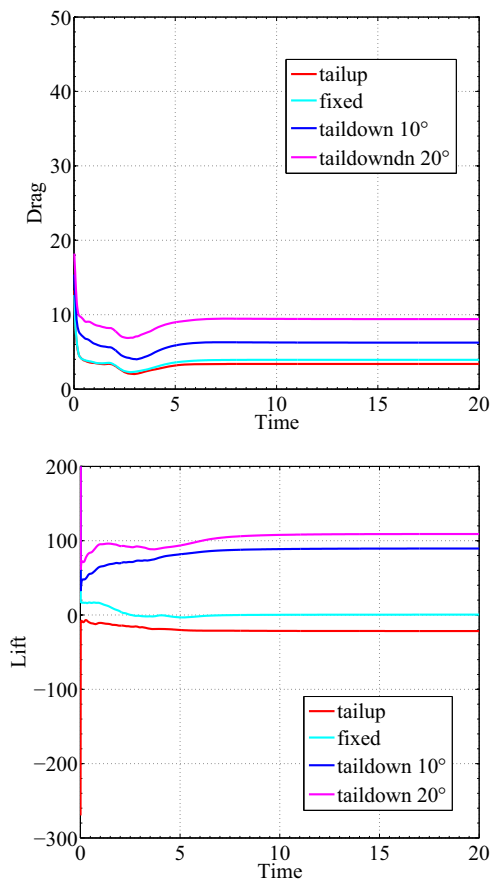
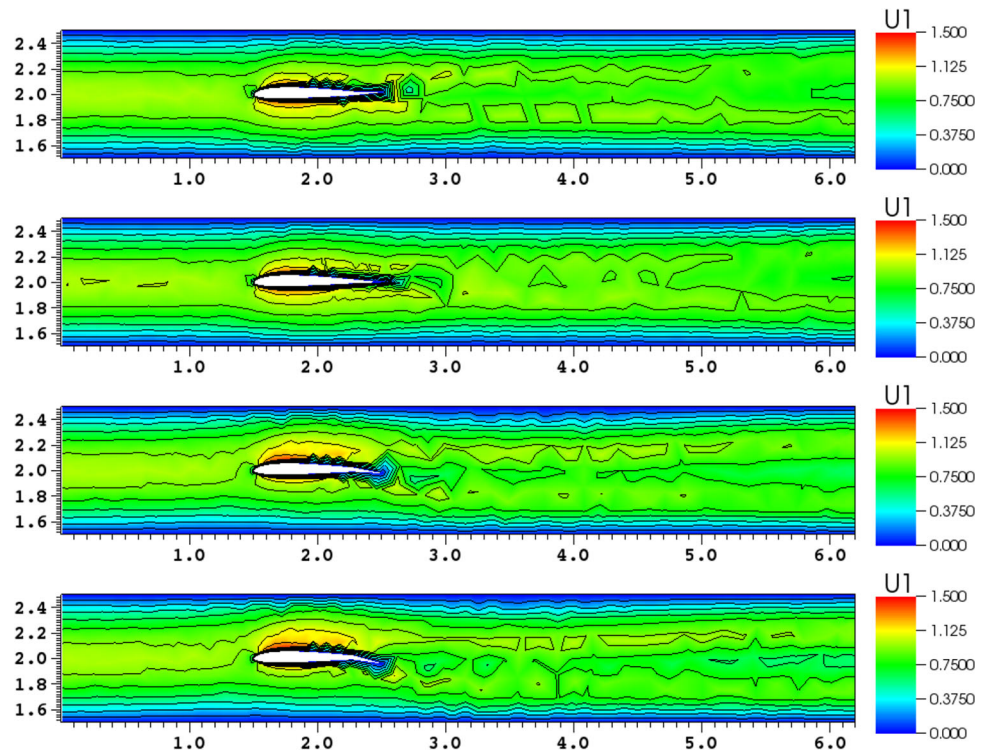


Fig. 12 The drag and the lift generated by the flow over different variants of the aerofoil SD 7003

6 Summary

Variational multiscale finite element simulation of turbulent flows over different variants of aerofoil are presented. In particular, the Smagorinsky eddy viscosity model is used in the VMS method. The numerical results for flow over a cylinder and different variants of NACA24012 and SD7003 aerofoils are presented. The drag and lift for the different variants are also computed.

References

1. Davidson, P.A.: Turbulence: An Introduction for Scientists and Engineers. Oxford University Press, Oxford (2004)
2. Pope, S.B.: Turbulent Flows. Cambridge University Press, Cambridge (2000)
3. Chen, H.C., Patel, V.C., Ju, S.: Solutions of Reynolds-averaged Navier–Stokes equations for three-dimensional incompressible flows. *J. Comput. Phys.* **88**, 305–336 (1990)
4. Fischer, P., Iliescu, T.: Large eddy simulation of turbulent channel flows by the rational les model. *Phys. Fluids* **15**, 3036–3047 (2003)
5. Guermund, J.L., Oden, J.T., Prudhomme, S.: Mathematical perspectives on large eddy simulation models for turbulent flows. *J. Math. Fluid Mech.* **6**, 194–248 (2004)
6. Rogallo, R.S., Moin, P.: Numerical simulation of turbulent flows. *Ann. Rev. Fluid Mech* **16**, 99–137 (1984)
7. Sagaut, P.: Large Eddy Simulation for Incompressible Flows, 2nd edn. Springer, Berlin (2002)
8. Hughes, T.J.R.: Multiscale phenomena: green’s functions, the dirichlet to neumann formulation, subgrid scale models, bubbles

- and origins of stabilized methods. *Comput. Methods Appl. Mech. Eng.* **127**, 387–401 (1995)
9. Hughes, T.J.R., Feijoo, G.R., Mazzei, L., Quincy, J.B.: The variational multiscale method—a paradigm for computational mechanics. *Comput. Methods Appl. Mech. Eng.* **166**, 3–24 (1998)
 10. Collis, S.S.: Monitoring unresolved scales in multiscale turbulence modelling. *Phys. Fluids* **13**(6), 1800–1806 (2001)
 11. Gannitizer, P., Gravemeier, V., Wall, W.A.: Advances in variational multiscale methods for turbulent flows. In: de Borst, R., Ramm, E. (eds.) *Multiscale Methods in Computational Mechanics. Lecture Notes in Applied and Computational Mechanics*, pp. 39–52. Springer, Berlin (2011)
 12. Gravemeier, V.: The variational multiscale methods for laminar and turbulent incompressible flows. Phd thesis, Institute of Structural Mechanics, University of Stuttgart (2003)
 13. John, V.: On large eddy simulation and variational multiscale methods in the numerical simulation of turbulent incompressible flows. *Appl. Math.* **51**(4), 321–353 (2006)
 14. John, V., Kaya, S., Layton, W.J.: A two-level variational multiscale method for convection-dominated convection diffusion equations. *Comput. Methods Appl. Mech. Eng.* **195**, 4594–4603 (2006)
 15. John, V., Layton, W.J.: Subgrid scale eddy viscosity models and variational multiscale methods. Technical report TR-MATH 03–05. University of Pittsburgh (2003)
 16. John, V., Kaya, S.: Finite element error analysis of a variational multiscale method for Navier–Stokes equations. *Adv. Comp. Math.* **28**, 43–61 (2008)
 17. John, V.: Large Eddy Simulation of Turbulent Incompressible Flows. Analytical and Numerical Results for a Class of LES Models. *Lecture Notes in Computational Science and Engineering*. Springer, Berlin (2004)
 18. Gannitizer, P., Gravemeier, V., Wall, W.A.: Time-dependent subgrid scales in residual-based large eddy simulation. *Comput. Methods Appl. Mech. Eng.* **199**, 819–827 (2010)
 19. Hughes, T.J.R., Mazzei, L., Jensen, K.E.: Large eddy simulation and variational multiscale methods. *Comput. Vis. Sci.* **3**, 47–59 (2000)
 20. Hughes, T.J.R., Oberai, A.A., Mazzei, L.: Large eddy simulation of turbulent channel flows by the variational multiscale method. *Phys. Fluids* **13**(6), 1784–1799 (2001)
 21. Gravemeier, V., Wall, W.A., Ramm, E.: A three level finite element method for instationary incompressible Navier–Stokes equations. *Comput. Methods Appl. Mech. Eng.* **193**, 1323–1366 (2004)
 22. Gravemeier, V., Wall, W.A., Ramm, E.: Large eddy simulation of turbulent incompressible flows by a three-level finite element method. *Int. J. Numer. Methods Fluids* **48**, 1067–1099 (2005)
 23. Masud, A., Calderer, R.: A variational multiscale method for incompressible turbulent flows: bubble functions and fine scale fields. *Comput. Methods Appl. Mech. Eng.* **200**, 2577–2593 (2011)
 24. John, V., Kaya, S.: A finite element variational multiscale method for the Navier–Stokes equation. *SIAM J. Sci. Comput.* **26**(5), 1485–1503 (2005)
 25. Gravemeier, V.: Scale-seperating operators for variational multiscale large eddy simulation of turbulent flows. *J. Comput. Phys.* **212**, 400–435 (2006)